Coordinated Feedback Power Control Method for Hybrid Multi-infeed HVDC System

Jiachen Zhang, Qi Xie, Zixuan Zheng, Chunyi Guo, Yi Zou, and Jie Ren

***Abstract*—During the power modulation process of line commutated converter-based high-voltage direct current (LCC-HVDC), the transient power mismatch between the fast-change converter station and the slow-response reactive power compensators (RPCs) can cause transient voltage disturbances at the weak sending end of the AC grid. To mitigate such voltage disturbances, this paper proposes a coordinated feedback power control method for the hybrid multi-infeed HVDC (HMI-HVDC) system comprising an LCC-HVDC and voltage source converter-based HVDC (VSC-HVDC) systems. The mechanism of the disturbance caused by transient power mismatch is quantitatively analyzed, and the numerical relationship between the instantaneous unbalanced power and the AC voltage is derived. Based on the numerical relationship and considering the time-varying relationship of reactive power between converter stations, the unbalanced power is set as the feedback and coordinately distributed among the inverter stations of VSC-HVDC, and the rectifier and the inverter stations of LCC-HVDC. Simulation results verify that the proposed method can effectively suppress voltage disturbance without relying on remote communication, thus enhancing the operation performance of the HMI-HVDC system.**

***Index Terms*—Coordinated control, line commutated converter-based high-voltage direct current (LCC-HVDC), sending end system, voltage disturbance, voltage source converter-based HVDC.**

I. Introduction

TRANSMITTING via line commutated converter-based high-voltage direct current (LCC-HVDC) systems is one of the most effective methods to accommodate large-scale onshore renewable energy, where power modulation is the primary method to deal with the intrinsic fluctuation of renewable energy [1], [2]. However, the reactive power consumed by the rectifier of an LCC-HVDC system varies rapidly with changes in the DC power, whereas the conventional mechanical switched filters exhibit slow responses, leading to mismatches in the transients of the reactive power during the switching processes of power modulations, inducing transient AC voltage disturbances. Moreover, the low short circuit ratio (SCR) of the sending end system exacerbates the disturbance and could even result in system voltage instability [3]-[6].

LCC-HVDC possesses weaknesses such as prone to commutation failure [7]-[9], whereas voltage source converter-based HVDC (VSC-HVDC) can provide rapid reactive power support to mitigate transient AC voltage disturbances on the rectifier side of the LCC-HVDC system [10]. Thus, the construction of a hybrid multi-infeed HVDC (HMI-HVDC) system comprising a VSC-HVDC system and an LCC-HVDC system, where renewable energy is locally collected by VSC-HVDC system and subsequently transmitted over a long distance via the LCC-HVDC system, has emerged as a promising solution for large-scale renewable energy exploitation [11]-[15]. For instance, the Chongqing-Hubei back-to-back project which forms a hybrid HVDC system with the Longzheng HVDC rectifier station, is in operation in China [16], [17]. Unlike point-to-point HVDC transmission, the inter-HVDC dynamic interactions impart HMI-HVDC systems with greater potential to mitigate AC voltage disturbances while presenting greater challenges to the system operation and control [18]-[21]. To suppress the voltage disturbance, it is important to ensure that the two HVDCs system do not interact negatively in any scenario. Additionally, a higher control burden and lower efficiency are obtained by adjusting just one controllable device. Therefore, the coordination between LCC-HVDC system and VSC-HVDC system is necessary and emphasized.

To mitigate the AC voltage disturbance in the HMI-HVDC system, measures for mitigating the AC voltage disturbance in the HMI-HVDC system can be implemented from either the LCC-HVDC side or the VSC-HVDC side. Measures on the LCC-HVDC side can be further divided into installing additional equipment and modifying the existing control strategies for LCC-HVDC systems. Measures on the VSC-HVDC side focus on modifying the existing reactive power decoupling outer-loop control strategy.

Conventional methods involve installing additional reactive power compensation equipment such as a static var compensator (SVC) and a static compensator (STATCOM) [22], [23], at LCC-HVDC rectifier stations. However, such methods incur further costs. Without adding additional costs,

Manuscript received: August 21, 2023; revised: January 4, 2024; accepted: April 2, 2024. Date of CrossCheck: April 2, 2024. Date of online publication: May 3, 2024.

This work was supported in part by the State Key Laboratory of Alternate Electrical Power System with Renewable Energy Sources (No. LAPS23020).

J. Zhang, Q. Xie, Z. Zheng (corresponding author), Y. Zou, and J. Ren are with the College of Electrical Engineering, Sichuan University, Chengdu 610065, China (e-mail: jiachen_zhang0921@163.com; xieqi365@outlook.com; scuzzx@163.com; 649532146@qq.com; renjieholmesjay@163.com).

C. Guo is with the State Key Laboratory for Alternate Electrical Power System with Renewable Energy Sources, North China Electric Power University, Beijing 102206, China (e-mail: chunyiguo@outlook.com).

DOI: 10.35833/MPCE.2023.000586

methods by controlling the reactive power consumption to adjusting the DC voltage have been proposed in [24], [25]. However, it is widely acknowledged that the dynamic voltage support capability under transient conditions is limited owing to its thyristor-based principle and the nature of the coupled active and reactive power control. Adjusting the reactive power output of the LCC-HVDC rectifier as desired using LCC-HVDC transmission alone affects the normal operation of the system and increases the regulatory burden of the system.

On the VSC-HVDC side, [26] proposes reactive power/voltage droop control strategies for VSCs connected to renewable energy sources to suppress power fluctuation disturbances. Reference [12] improves the transient characteristics of LCC-HVDC by feeding back the difference of transmitted reactive power between VSC-HVDC and LCC-HVDC after commutation failures to the constant AC voltage control of VSC-HVDC using a proportional-integral (PI) controller. In [27], a collaborative reactive power control strategy with VSC-HVDC and filter coordination is proposed to reduce LCC-HVDC filter switching, essentially feeding back the reactive power compensation value to VSC-HVDC using a PI controller. Reference [28] aims to suppress transient low- and over-voltages by calculating the reactive power compensation value based on the slope of the firing angle of the LCC-HVDC rectifier after a commutation failure. Although these strategies utilize the VSC to improve system stability, the potential for coordinated regulation between VSC-HVDC and LCC-HVDC has not been fully exploited. Considering that the capacity of VSC-HVDC is significantly lower than that of LCC-HVDC, which limits the adjustment capabilities of a single DC regulation resource, higher control burden and lower efficiency are observed by just adjusting VSC-HVDC. In addition, existing control strategies, while incorporating given supplementary control instructions, are mostly based on PI controllers for qualitative control, which lack quantitative analysis of the control instructions. The effectiveness of these control methods requires further enhancement.

In this paper, we derive a quantitative relationship between unbalanced power and AC voltage based on mechanism analysis of the transient AC voltage disturbances at the sending end of the grid during the switching process of LCC-HVDC power modulation. Moreover, we propose a coordinated feedback power control method for HMI-HVDC that aims to mitigate the sending end AC voltage disturbance during the switching process of LCC-HVDC power modulation. In the proposed method, considering the time-varying relationship of reactive power between converter stations, unbalanced power is designated as the feedback and is coherently distributed among the multiple controllable resources to achieve mutually reinforcing control effects. The proposed method can be used to achieve a lower control burden and higher control efficiency without relying on remote communication.

The remainder of this paper is organized as follows. Section II presents mechanism analysis of the AC voltage disturbance at LCC-HVDC sending end. Section III proposes the coordinated control method. Section IV verifies the method with simulations. Finally, Section V concludes the paper.

II. Mechanism Analysis of AC Voltage Disturbance at LCC-HVDC Sending End

A. Brief Descriptions of HMI-HVDC System

A typical HMI-HVDC system is shown in Fig. 1, where the part of renewable power is gathered to the point of common coupling (PCC) through VSC-HVDC. The power is then transmitted over long distances to load centers via the large-capacity LCC-HVDC system, along with other large-scale wind power gathered through AC lines.

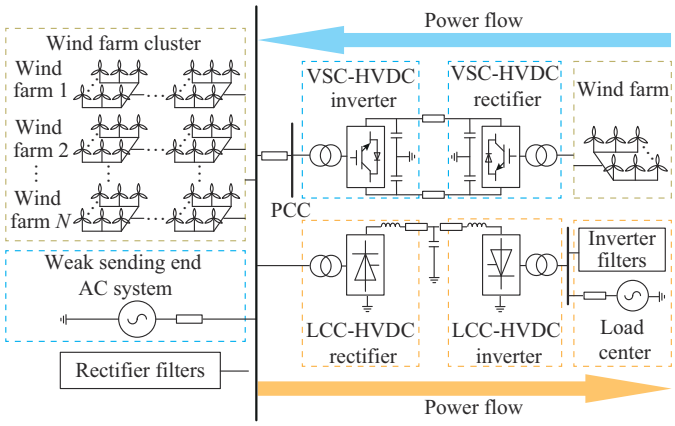

Fig. 1. Typical HMI-HVDC system.

B. Mechanism of AC Voltage Disturbances Caused by Transient Power Mismatch

Considering that LCC-HVDC transmission power changes quickly during the switching process of HVDC power modulation, the inherent randomness and volatility of wind power invariably result in significant fluctuations in LCC-HVDC power transmission. Consequently, a recurrent switching of traditional reactive power compensation devices occurs. This frequent switching increases the wear and tear of the equipment, thereby diminishing its lifespan [29]. Furthermore, the mechanical switching device of reactive power compensation usually equipped in LCC-HVDC has a long switching process. Generally, the switching process of the mechanical fixed capacitor usually sustains 200 ms [30]. Consequently, when variations in transmission power occur, both the transmitted active power and the consumed reactive power alter, whereas the reactive power compensation devices continue to generate the reactive power required prior to the power change, owing to their extended switching process. This disjunction in reactive power results in voltage disturbances at the PCC, which could trigger voltage stability problems, further exacerbating the challenges already faced due to the dynamic nature of the power generation sources.

To simplify the analysis, an equivalent circuit that corresponds to Fig. 1 is established, as shown in Fig. 2. Utilizing the Thevenin equivalent method, the entire sending end AC system including wind farms is represented by a voltage source with a reactance. AC filters and reactive compensators are represented by an equivalent capacitor.

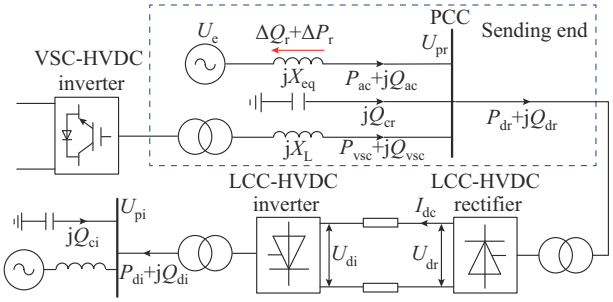

Fig. 2. Simplified equivalent circuit for analysis.

As shown in Fig. 2, U_e, U_{pr}, and U_{pi} are the equivalent voltage of the AC system, AC voltage at the PCC, and AC voltage on the LCC-HVDC inverter side, respectively; U_{dr} and U_{di} are the DC voltages on the LCC-HVDC rectifier and inverter sides, respectively; I_{dc} is the DC current of LCC; P_{ac} and Q_{ac} are the active power and reactive power provided by the AC system, respectively; P_{vsc} and Q_{vsc} are the active power and reactive power transmitted by VSC-HVDC, respectively; P_{dr} and Q_{dr} are the active power and reactive power consumed by the LCC-HVDC rectifier station, respectively; P_{di} and Q_{di} are the active power and reactive power consumed by the LCC-HVDC inverter station, respectively; Q_{cr} and Q_{ci} are the reactive power provided by the rectifier station filters and the inverter station filters, respectively; X_{eq} is the equivalent reactance of AC system; X_L is the equivalent reactance of tie line; and ΔP_r and ΔQ_r are the unbalanced active power and unbalanced reactive power injected into the AC system, respectively.

The power relationships of AC and DC systems are:

$$P_{dr}=P_{ac}+P_{vsc} \tag{1}$$

$$Q_{dr}=Q_{ac}+Q_{cr}+Q_{vsc} \tag{2}$$

Generally, ΔP_r and ΔQ_r shown in Fig. 2 are both zero. Assuming that VSC-HVDC maintains constant active and reactive power control operation, when the transmission power of LCC-HVDC changes, ΔP_r and ΔQ_r will change accordingly owing to the variations of P_{dr} and Q_{dr}. Therefore, U_{pr} will deviate from the rated value and can be calculated by U_{prN}. ΔP_r and ΔQ_r are defined as follows:

$$\Delta P_r=P_{acN}-P_{ac}=P_{acN}-P_{dr}+P_{vsc} \tag{3}$$

$$\Delta Q_r=Q_{acN}-Q_{ac}=Q_{acN}-Q_{dr}+Q_{cr}+Q_{vsc}-\Delta Q_1 \tag{4}$$

where the subscript N indicates the value under normal conditions; and ΔQ_1 is the reactive power loss on the equivalent reactance of the AC system, assuming that the filter does not react owing to its inherent delay.

Q_{cr} and ΔQ_1 can be expressed as:

$$Q_{cr}=\left(\frac{U_{pr}}{U_{prN}}\right)^2 Q_{cN} \tag{5}$$

$$\Delta Q_1=\frac{(P_{ac}+jQ_{ac})^2}{U_{pr}^2}X_{eq} \tag{6}$$

Then, U_{pr} can be derived as:

$$U_{pr}=\sqrt{\left(U_{prN}+\frac{\Delta Q_r X_{eq}}{U_{prN}}\right)^2+\left(\frac{\Delta P_r X_{eq}}{U_{prN}}\right)^2} \tag{7}$$

U_{pr} can be calculated by solving the above equations. Our previous work has revealed that both ΔQ_r and ΔP_r lead to variations in U_{pr}, whereas the former is the dominant factor, and the variation of Q_{dr} is the direct cause of the unbalanced power exchange between the sending end AC system and the HVDC system during the change of transmission power. P_{dr} also has some minor effects. Therefore, the analysis of the AC voltage disturbance should focus on the change of Q_{dr}. Based on the quasi-steady state model of LCC-HVDC [31], Q_{dr} can be expressed as:

$$Q_{dr}=I_{dc}\left[\frac{18}{\pi^2}N^2T^2U_{pr}^2(1-\cos^2\alpha)-\frac{9}{\pi^2}N^2X_{r1}^2I_{dc}^2+\frac{18\sqrt{2}}{\pi^2}N^2TU_{pr}\cos\alpha X_{r1}I_{dc}\right]^{\frac{1}{2}} \tag{8}$$

where N is the number of six pulse converters; T is the turn ratio of the converter transformer; α is the firing angle of the rectifier station; and X_{r1} is the commutation reactance of the rectifier.

Equation (8) reveals that Q_{dr} is primarily determined by I_{dc} and α. The equation implies that Q_{dr} is almost proportional to I_{dc} and the relationship between α and Q_{dr} follows a cosine function [32]. When the LCC-HVDC transmission power increases, the increase in P_{dr} induces a negative ΔP_r, and concurrently, the increased I_{dc} results in a higher Q_{dr}, thereby causing a negative ΔQ_r. The combined effect of ΔQ_r and ΔP_r contributes to a decrease in U_{pr}. Similarly, when the transmission power decreases, the combination of ΔQ_r and ΔP_r ultimately increases U_{pr}. In essence, the fundamental strategy to mitigate AC voltage disturbances at the sending end revolves around eliminating the power imbalance within the HMI-HVDC system.

III. Proposed Coordinated Control Method

A. Overall Principle of Coordinated Control Method

As renewable energy installations expand, substantial impacts on the grid, potentially unmanageable for individual regional grids, could arise from large-scale renewable power. However, these impacts can be mitigated by dynamically adjusting the transmission power in real time to relocate the influence of renewable energy fluctuations to larger power grids, thereby ensuring grid stability and safety. Consequently, an effective strategy would involve utilizing all three controllable resources within the HMI-HVDC system, i.e., the inverter station of VSC-HVDC, and rectifier and inverter stations of LCC-HVDC, holistically to stabilize the unbalanced power between the sending end AC system and the HVDC system. By considering the time-varying relationship of reactive power between the controllable resources and leveraging the quantified relationship between unbalanced power and AC voltage, the proposed coordinated control method enables more efficient use of the available resources. This method not only reduces the control burden exerted on each

resource but also contributes to improving the resiliency of the overall system. More importantly, this comprehensive strategy improves the system capacity to suppress voltage disturbances, thereby more effectively addressing the primary problem at hand. Accordingly, the proposed method optimizes resource utilization and system performance simultaneously. The flowchart of the proposed method is illustrated in Fig. 3.

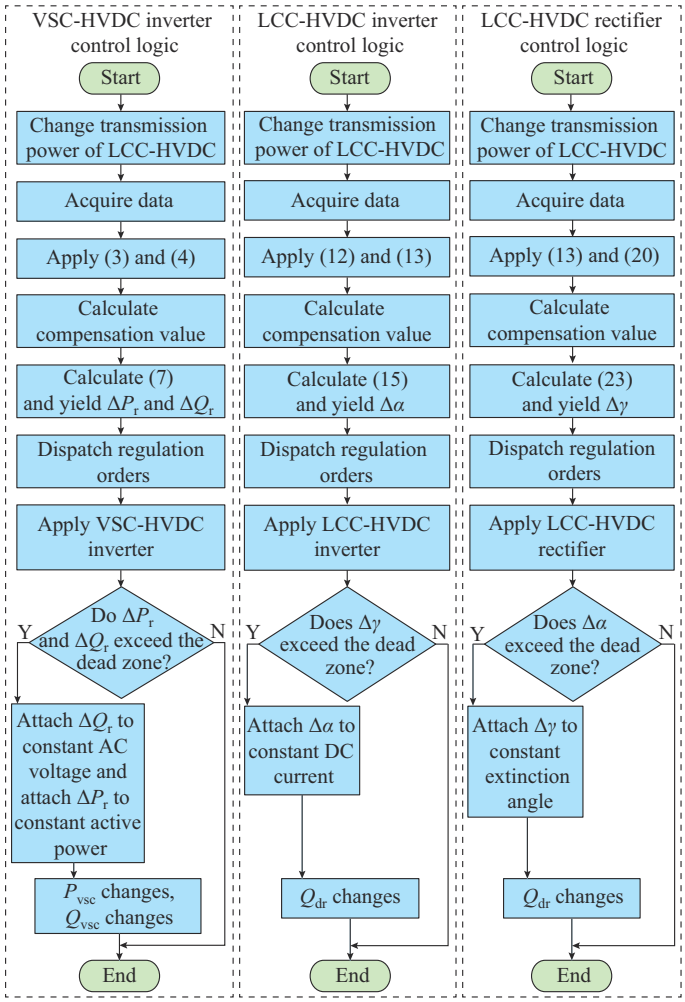

Fig. 3. Flowchart of proposed method.

Considering the time-varying relationship of reactive power between the converter stations, the unbalanced reactive power, as defined in (4), is the difference between the reactive power provided by the filters and the reactive power consumed by the LCC-HVDC rectifier station. To address the imbalances in reactive power, the reactive power compensation value, as determined by (7), is fed back to the reactive power control of the VSC-HVDC inverter station. This enables the absorption of excessive reactive power supplied by the filter, while also compensating for the reactive power that the filter fails to supply. Second, a compensation value for α is calculated using the relationship between Q_{dr} and α, as delineated in (8). The value is then fed back to the constant direct current control of the LCC-HVDC rectifier station, facilitating Q_{dr} to gravitate toward its value preceding the change in transmission power. This strategy not only alleviates the control burden imposed on the VSC-HVDC owing to capacity constraints, but also enhances the speed and efficacy of the control response.

Additionally, for conventional control strategies, the LCC-HVDC inverter maintains the extinction angle γ at a specific value regardless of the changes in the reactive power demand. Therefore, if the LCC-HVDC is to further enhance the AC voltage support of the rectifier side, fast communication between both ends is required, which increases implementation costs and reduces system reliability. By adjusting the DC voltage, we can control the reactive power consumption of the LCC-HVDC rectifier station. This objective is achieved by calculating the compensation value for γ using local power change information and then feeding it back to the constant extinction angle control of the LCC-HVDC inverter station. Such adjustment enables the regulation of DC voltage, and consequently, the control of Q_{dr}. Collectively, regulating Q_{dr} by simultaneously leveraging α and γ results in the optimized use of power regulation resources. In addition to alleviating the regulatory burden on Q_{dr} in the LCC-HVDC rectifier station, it also enhances control performance.

In addressing the imbalances in active power, the active compensation value, determined according to (7), is calculated and fed back to the active power control of the VSC-HVDC inverter station, thereby mitigating the unbalanced active power.

Based on the aforementioned analysis, the proposed method comprehensively employs multiple controllable resources, as shown in Fig. 4, including the unbalanced power quantitative feedback control at the VSC-HVDC inverter station, the firing angle quantitative feedback control at the LCC-HVDC rectifier station, and the extinction angle quantitative feedback control at the LCC-HVDC inverter station.

B. Unbalanced Power Quantitative Feedback Control of VSC-HVDC Inverter Station

Unlike LCC-HVDC, VSC-HVDC can achieve the decoupling control of active and reactive power. As illustrated in Fig. 4, the VSC-HVDC inverter station adopts constant active power control and constant AC voltage control, where U_{ac} and U_{acref} are the measured and reference values of the AC voltage at PCC, respectively; P and P_{ref} are the measured and reference values of the VSC-HVDC active power, respectively; i_{qref} and i_{dref} are the reference values of reactive current and active current of the inner loop control in VSC-HVDC, respectively.

The constituents of ΔP_r and ΔQ_r, namely the active and reactive quantities, can be captured in real time at the connection point of the VSC-HVDC inverter station and subsequently be fed back to the outer loop control of the VSC-HVDC system via telecommunication networks. First-order filters are utilized to address potential measurement delays and ensure continuity of the measured values.

To avoid frequent actions of the proposed method, upper and lower dead zones, ΔQ^H and ΔQ^L, respectively, are established. When ΔQ_r exceeds the boundaries of the dead zone $[\Delta Q^H, \Delta Q^L]$, switch A is engaged. Subsequently, the AC voltage compensation value, corresponding to ΔQ_r and determined by its relationship with the AC voltage at PCC per

(7), is fed back to the constant AC voltage control. Simultaneously, ΔP_r is incorporated into the constant active power control. The quantitative incorporation of both ΔQ_r and ΔP_r significantly enhances the response rates of i_{qref} and i_{dref}, optimizing the use of VSC-HVDC for suppressing transient power imbalances.

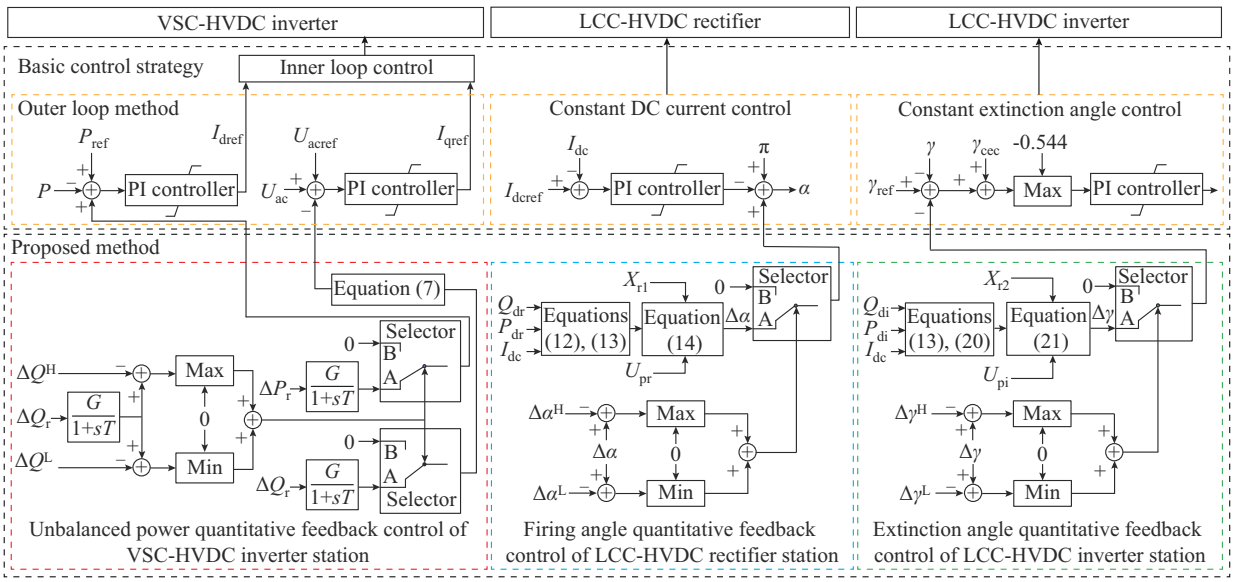

Fig. 4. Overall block diagram of coordinated power control method for HMI-HVDC system.

C. Firing Angle Quantitative Feedback Control of LCC-HVDC Rectifier Station

According to (8), the relationship between α and Q_{dr} follows a cosine function, with an initial operation state of $\alpha = 17°$. During a decrease in LCC-HVDC transmission power, an overcompensation of reactive power arises from the combined effects of Q_{dr} reduction and filter action delay. By increasing α, Q_{dr} can be increased, thereby absorbing a portion of the surplus reactive power. Conversely, in the event of an increase in LCC-HVDC transmission power, under-compensation of reactive power by the filter can be avoided by decreasing α, thus reducing Q_{dr}. The strategy significantly enhances the reliability and stability of the power system by ensuring a more balanced reactive power distribution during fluctuations in transmission power.

According to the quasi-steady state model of LCC-HVDC, the following relationships can be obtained:

$$Q_{dr} = P_{dr} \tan \varphi_r = P_{dr} \sqrt{\frac{1}{\cos^2 \varphi_r} - 1} \tag{9}$$

$$\cos \varphi_r = \frac{U_{dr}}{U_{d0r}} = \cos \alpha - \frac{X_{r1} I_{dc}}{\sqrt{2}\, T U_{pr}} \tag{10}$$

where U_{d0r} and φ_r are the open-circuit DC voltage and power factor angle on the rectifier side, respectively.

From (9) and (10), the numerical relationship between α and Q_{dr} can be derived as:

$$\alpha = \arccos\left\{ \sqrt{1 \Big/ \left[\left(\frac{Q_{dr}}{P_{dr}} \right)^2 + 1 \right]} + \frac{X_{r1} I_{dc}}{\sqrt{2}\, T U_{pr}} \right\} \tag{11}$$

When the transmission power changes, the following relationship is satisfied.

$$\begin{cases} \Delta P_{dr} = P_{drN} - P_{dr} \\ \Delta Q_{dr} = Q_{drN} - Q_{dr} \end{cases} \tag{12}$$

$$\Delta I_{dc} = I_{dcN} - I_{dc} \tag{13}$$

Combining (11), the feedback value of the firing angle can be expressed as (14), which is fed back to the constant DC current control of the LCC-HVDC rectifier station, as shown in Fig. 4, where I_{dc} and I_{dcref} are the measured and reference values of DC current, and $\Delta\alpha^H$ and $\Delta\alpha^L$ are the upper and lower firing angle limits of the dead zone, respectively.

$$\Delta\alpha = \arccos\left\{ \sqrt{1 \Big/ \left[\left(\frac{\Delta Q_{dr}}{\Delta P_{dr}} \right)^2 + 1 \right]} + \frac{X_{r1} \Delta I_{dc}}{\sqrt{2}\, T U_{pr}} \right\} \tag{14}$$

The control method enables the adjustment of α according to the measured value of the reactive power consumption on the rectifier side of the LCC-HVDC, and thus the burden at the VSC-HVDC inverter station to regulate reactive power can be relieved, which enables the further improvement of the performance on unbalanced power suppression.

D. Extinction Angle Quantitative Feedback Control of LCC-HVDC Inverter Station

Despite the contribution of adjusting α in the LCC rectifier station to the suppression of unbalanced power, in the context of the HVDCs connected to weak grids, where the AC voltage fluctuates sensitively based on the active power and reactive power of the HVDC, the controllable range of reactive power is finite because the extent of α variation must be limited to prevent HVDC malfunction. Furthermore, adjusting other relevant parameters of the rectifier station would escalate the regulatory burden and potentially push α beyond an acceptable range. Further work to control the reactive power of the LCC rectifier connected to a weak grid is need-

ed, thereby reducing the power regulatory burden of the LCC-HVDC rectifier station and extending the regulation range.

The DC current of the LCC-HVDC system can be expressed as:

$$I_{dc}=\frac{U_{dr}-U_{di}}{R} \tag{15}$$

where R is the DC circuit resistance. From (8) and (15), I_{dc} is almost proportional to Q_{dr}, and it is also proportional to the difference ΔU between U_{dr} and U_{di}. When variations occur in the LCC-HVDC transmission power, U_{dr} and U_{di} exhibit similar trends but with varying magnitudes of change. As previously mentioned, the LCC-HVDC inverter station adopts constant extinction angle control, enabling the regulation of the DC voltage by adjusting γ. Consequently, ΔU can be controlled through this manipulation. The reactive power consumption can be effectively regulated by adjusting γ through a numerical relationship.

Furthermore, the regulation of reactive power via controlling γ at the LCC-HVDC inverter station not only reduces the regulatory burden at the rectifier station but also broadens the range of adjustment for unbalanced power, effectively utilizing the existing controllable resources. Further improvement in the suppression effect on unbalanced power is achievable through the coordinated adjustment of α and γ. Simultaneously, it ensures that system operation parameters such as DC voltage remain within acceptable ranges.

In the context of the LCC-HVDC inverter station, the following relationships can be derived:

$$U_{d0i}=\frac{3\sqrt{2}}{\pi}NTU_{pi} \tag{16}$$

$$U_{di}=U_{d0i}\cos\gamma-\frac{3}{\pi}X_{r2}NI_{dc} \tag{17}$$

where U_{d0i} is the open-circuit DC voltage on the inverter side; and X_{r2} is the commutation reactance of the inverter station.

Considering the communication delay between the LCC-HVDC rectifier and inverter stations, the quantitatively calculated feedback value of γ relies on local information gathered at the inverter station. Subsequently, the following relationships are established.

$$Q_{di}=P_{di}\tan\varphi_i=P_{di}\sqrt{\frac{1}{\cos^2\varphi_i}-1} \tag{18}$$

$$\cos\varphi_i=\frac{U_{di}}{U_{d0i}}=\cos\gamma-\frac{X_{r2}I_{dc}}{\sqrt{2}\,TU_{pi}} \tag{19}$$

$$\begin{cases}\Delta P_{di}=P_{diN}-P_{di}\\ \Delta Q_{di}=Q_{diN}-Q_{di}\end{cases} \tag{20}$$

where φ_i is the power factor angle of the inverter station.

From (18)-(20), the quantitative feedback value for the extinction angle can be articulated as in (21). The value is subsequently appended to the constant extinction angle control at the LCC-HVDC inverter station, as shown in Fig. 4, where γ_{ref} is the reference value of the extinction angle; γ_{cec} is the output value of the current error controller; and $\Delta\gamma^H$ and $\Delta\gamma^L$ are the upper and lower thresholds of the action dead zone for the extinction angle, respectively.

$$\Delta\gamma=\arccos\left\{\sqrt{1\Big/\left[\left(\frac{\Delta Q_{di}}{\Delta P_{di}}\right)^2+1\right]}+\frac{X_{r2}\Delta I_{dc}}{\sqrt{2}\,TU_{pi}}\right\} \tag{21}$$

When the transmitted power changes, if $\Delta\gamma$ exceeds the upper or lower thresholds of the action dead zone, it is fed back to the constant extinction angle control to expedite the regulation of Q_{dr} by the LCC-HVDC inverter station.

IV. Simulation Results

A. Simulation Conditions

A test system, as illustrated in Fig. 1, is constructed in PSCAD/EMTDC to support the research and verify the validity and superiority of the proposed method. The parameters of LCC-HVDC and VSC-HVDC are detailed in Appendix A Table AI. Sending end AC systems, including wind farms, are represented according to Thevenin's theorem [31], [32]. Under Thevenin equivalent, the output power of the AC system can undergo instantaneous changes. Most wind farms in the real world are located at outlying weak AC systems, whose SCR is generally less than 3 [33]. The SCR of the AC system connected to the LCC is set to be 2.5, which is a weak grid. The changes in LCC-HVDC operation conditions during the switching process of power modulation are simulated by adjusting the LCC-HVDC DC current order. Considering that the reactive power of the system fluctuates during stable operation, $\Delta Q^H=20$ Mvar and $\Delta Q^L=-20$ Mvar. According to [34], $[\Delta\alpha^H,\Delta\alpha^L]$ is set to be $[2.5°,-2.5°]$ and $[\Delta\gamma^H,\Delta\gamma^L]$ is set to be to $[1°,-1°]$. The LCC-HVDC system is constructed based on the CIGRE benchmark [35], and VSC-HVDC is constructed according to [36], with both being detailed electromagnetic transient models.

In the proposed method, for the rectifier and inverter components of the LCC-HVDC, the feedback value for control is determined by utilizing locally available information. Regarding the inverter component of the VSC-HVDC within the proposed method, the feedback value for control is determined by the power information of the PCC. Given the minimal electrical distance that separates the VSC-HVDC inverter station from the LCC-HVDC rectifier station, the influence of communication delay is considered relatively insignificant. A first-order inertial link is established to simulate communication delay, marked by a proportionality factor G of 1.0 and a time factor T of 0.01 s.

To verify the effectiveness of the proposed method, the performance of the proposed method is compared with the other three methods under LCC-HVDC transmission power change.

1) Method A: VSC-HVDC reactive power control adopts constant reactive power control, and LCC-HVDC adopts default control.

2) Method B: VSC-HVDC reactive power control adopts constant AC voltage control, and LCC-HVDC reactive power control adopts default control.

3) Method C: VSC-HVDC adopts reactive power coordi-

nation control [12], and LCC-HVDC adopts default control.

4) Method D: proposed method.

Adjustments to the LCC-HVDC transmission power are performed by modulating I_{dc} in coordination with the operation of the transformer taps.

B. LCC-HVDC Transmission Power Decrease

In the scenario where the active power of DC transmission decreases following a decline in wind power, the DC current order of LCC-HVDC changes from 1.0 p.u. to 0.7 p.u. at $t=3$ s. The simulation results are shown in Fig. 5(a)-(i).

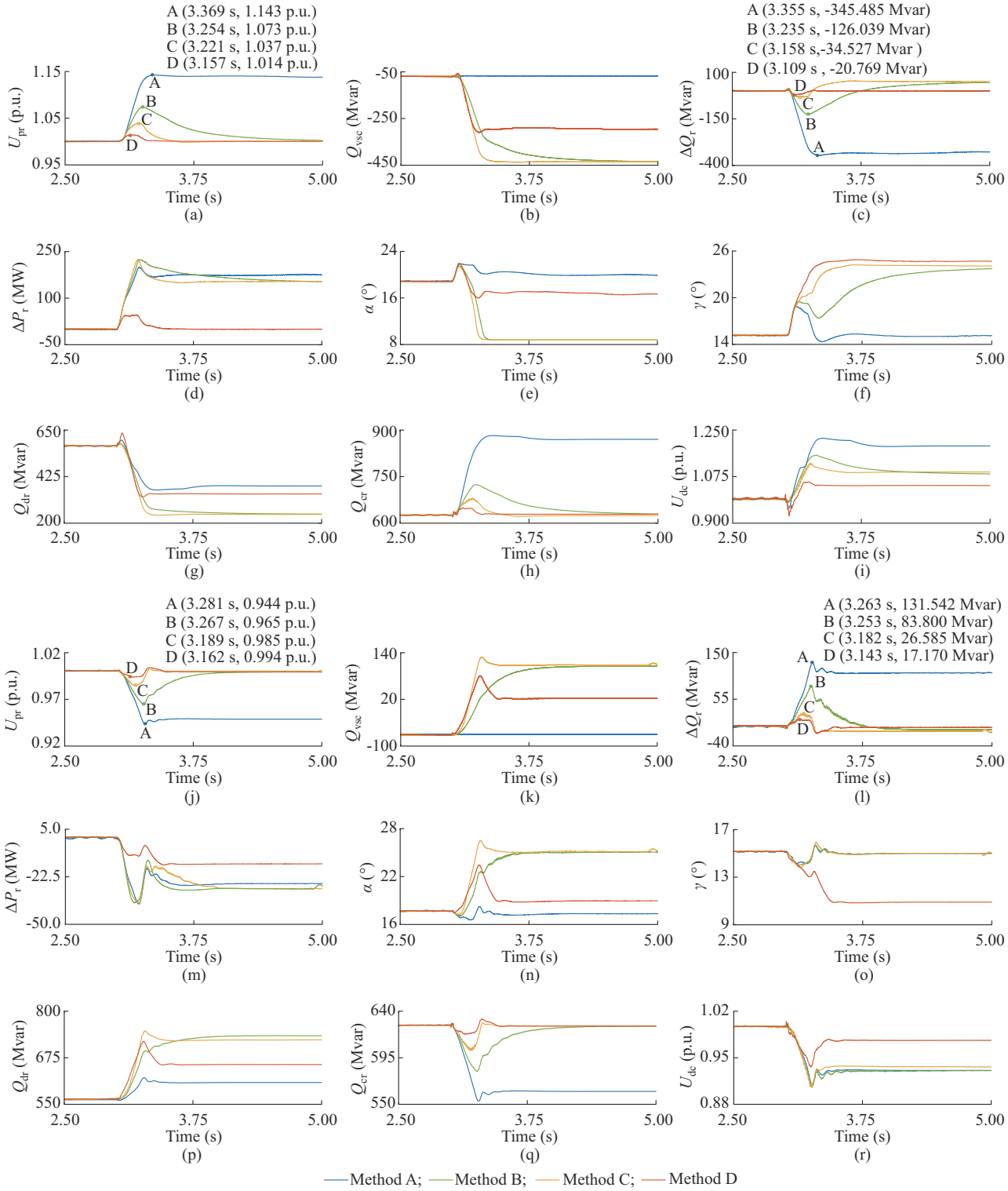

Fig. 5. Simulation results under LCC-HVDC transmission power change. (a) U_{pr} under power decrease. (b) Q_{vsc} under power decrease. (c) ΔQ_r under power decrease. (d) ΔP_r under power decrease. (e) α under power decrease. (f) γ under power decrease. (g) Q_{dr} under power decrease. (h) Q_{cr} under power decrease. (i) U_{dc} under power decrease. (j) U_{pr} under power increase. (k) Q_{vsc} under power increase. (l) ΔQ_r under power increase. (m) ΔP_r under power increase. (n) α under power increase. (o) γ under power increase. (p) Q_{dr} under power increase. (q) Q_{cr} under power increase. (r) U_{dc} under power increase.

The comparison of variables under power decrease is presented in Appendix A Table AII.

In terms of the control efficacy, it can be observed from Fig. 5(a), (c), and (d) that when the LCC-HVDC transmission power decreases, method A, which can be considered as the initial control, exhibits a maximum voltage of 1.143 p.u.. The minimum unbalanced reactive power reaches –345.485 Mvar. The imbalance in reactive power ΔQ_r at PCC is composed of Q_{dr}, which deviates from its normal operation rated value, and the excessive Q_{cr}, as shown in Fig. 5(g) and (h). According to Table AII, ΔQ_{dr} reaches 204.781 Mvar, and Q_{cr} reaches 882.268 Mvar. Meanwhile, U_{dc} increases as shown in Fig. 5(i). In method B, with the implementation of constant AC voltage control, once the voltage at PCC exceeds its rectified value due to unbalanced power, the VSC-HVDC inverter station absorbs excessive reactive power to suppress overvoltage. Method C accelerates the transmission rate of Q_{vsc} by attaching the difference of reactive power between VSC and LCC transmission via a PI controller based on method B. As a result, methods B and C decrease the maximum U_{pr} from 1.143 p.u. to 1.073 p.u. and 1.037 p.u., respectively, and the minimum value of unbalanced reactive power is enhanced from –345.485 Mvar to –126.039 Mvar and –34.530 Mvar, respectively. Furthermore, in method B, as shown in Fig. 5(g) and (h), under the slow recovery of AC voltage, Q_{cr} progressively decreases its excessive reactive power output to 724.071 Mvar. However, Q_{dr} deviates more from its rated value under normal operation Q_{drN} compared with the scenario where VSC-HVDC does not provide reactive power support, i.e., method A. This phenomenon is also observed with method C. As indicated in Table AII, ΔQ_{dr} reaches 321.070 Mvar and 326.484 Mvar, respectively. The proposed method D exhibits the best performance among all these methods, reducing the maximum voltage to 1.014 p.u., enhancing the minimum unbalanced reactive power value to –20.769 Mvar, and suppressing unbalanced active power. Moreover, this enables Q_{vsc} to dynamically interact with Q_{dr} and Q_{cr}. The increase in ΔQ_{dr} is effectively controlled, which reaches 238.056 Mvar. Additionally, Q_{cr} returns to its normal output more swiftly, which reaches 649.134 Mvar, and the increase in DC voltage is further decreased. It is evident that methods B, C, and D are more effective in suppressing the overvoltage compared with method A, but method D stands out by more precisely compensating for instantaneous unbalanced power.

In terms of the response speed, Table AII indicates that, compared with methods B and C, method D achieves shorter peak time for U_{pr}, specifically 3.157 s. Additionally, as shown in Fig. 5(b), method D results in a more rapid VSC-HVDC response in terms of absorbing reactive power, whereas the firing and extinction angles of LCC-HVDC are adjusted to the corresponding integer values faster during power transmission reductions. These results imply that method D can respond more rapidly to unbalanced power.

In terms of the integrated utilization of controllable resources, Fig. 5(b) demonstrates that, compared with methods B and C, method D requires VSC-HVDC to absorb less reactive power, thus reducing the burden of reactive power regulation. Furthermore, successful voltage disturbance suppression is attributable in part to the effective control over reactive power consumption at the LCC-HVDC rectifier station, which is closely tied to adjustments in the firing and extinction angles. As shown in Fig. 5(e) and (f), the firing angle at the LCC-HVDC rectifier station and the extinction angle at the LCC-HVDC inverter station are coordinated and controlled, being adjusted to the corresponding integer value based on a predefined numerical relationship. The adjustment enhances the reactive power consumption of the rectifier station while mitigating excessive drops in the firing angle to achieve the desired control effect. It can be observed that owing to the improved characteristics of Q_{dr}, the reactive power exchange between the sending end AC system and rectifier station is much smoother, confirming that method D can make comprehensive use of multiple controllable resources and reduce the power regulation burden at each converter station.

C. LCC-HVDC Transmission Power Increase

Under this condition, the DC current instruction for LCC-HVDC increases from 1.0 p.u. to 1.1 p.u. at $t=3$ s. The simulation results are shown in Fig. 5(j)-(r). A comparison of the variables under power increase is detailed in Appendix A Table AIII.

In terms of the control efficacy, as indicated in Fig. 5(j), (l), and (m), when the LCC transmission power increases, the minimum voltage for method A is 0.944 p.u., and the unbalanced reactive power reaches a maximum of 131.542 Mvar. ΔQ_r at the PCC is composed of the excessive Q_{dr} and the decreased Q_{cr}, as shown in Fig 5(p) and (q), respectively. It is evident from Table AIII that ΔQ_{dr} reaches –56.493 Mvar, and Q_{cr} reaches 552.167 Mvar. Meanwhile, U_{dc} decreases as shown in Fig. 5(r). Methods B and C increase this minimum voltage to 0.965 p.u. and 0.985 p.u., respectively, and decrease the maximum unbalanced reactive power to 83.800 Mvar and 26.585 Mvar, respectively. Q_{cr} values are increased to 581.670 Mvar and 604.940 Mvar, respectively. However, as indicated in Table AIII, ΔQ_{dr} reaches –169.552 Mvar and –199.800 Mvar, respectively. This creates a larger ΔQ_{dr}. As illustrated in Fig. 5(k), the VSC-HVDC inverter station has to generate more reactive power to support the LCC-HVDC rectifier station, thereby imposing a greater burden on its reactive power control. Similar to its performance during power reduction, method D outperforms other alternatives: it increases the minimum voltage to 0.994 p.u., and decreases the maximum unbalanced reactive power to 17.170 Mvar, concurrently suppressing unbalanced active power. Additionally, the decrease in ΔQ_{dr} is suppressed to –153.52 Mvar. Q_{cr} reaches 617.635 Mvar, and the drop in DC voltage is mitigated. Consequently, methods B, C, and D are more effective in mitigating the low voltage compared with method A, and it can be deemed that method D exhibits the best performance in suppressing the voltage disturbance.

In terms of response speed, as shown in Table AIII, compared with methods B and C, method D exhibits shorter peak time of 3.162 s for U_{pr}. Moreover, as indicated in

Fig. 5(k), method D yields faster reactive power responses from VSC-HVDC, alongside quicker adjustments to the corresponding setting values of firing and extinction angles of LCC-HVDC under power increase. This confirms that method D provides a faster response to unbalanced power under both power increase and decrease.

When LCC-HVDC transmission power increases, the analysis for the optimization of controllable resource usage is similar to the condition of power decrease, as shown in Fig. 8(k), (n), and (o), which will not be repeated here.

D. Analysis of Proposed Method at Different Fluctuation Magnitudes of LCC-HVDC Transmission Power

To further validate the effectiveness and applicability of method D at different fluctuation magnitudes of the LCC-HVDC transmission power, simulation analysis is performed for the above four methods with different degrees of power decrease and increase. The results are shown in Fig. 6, and the corresponding peak values are presented in Appendix A Table AIV.

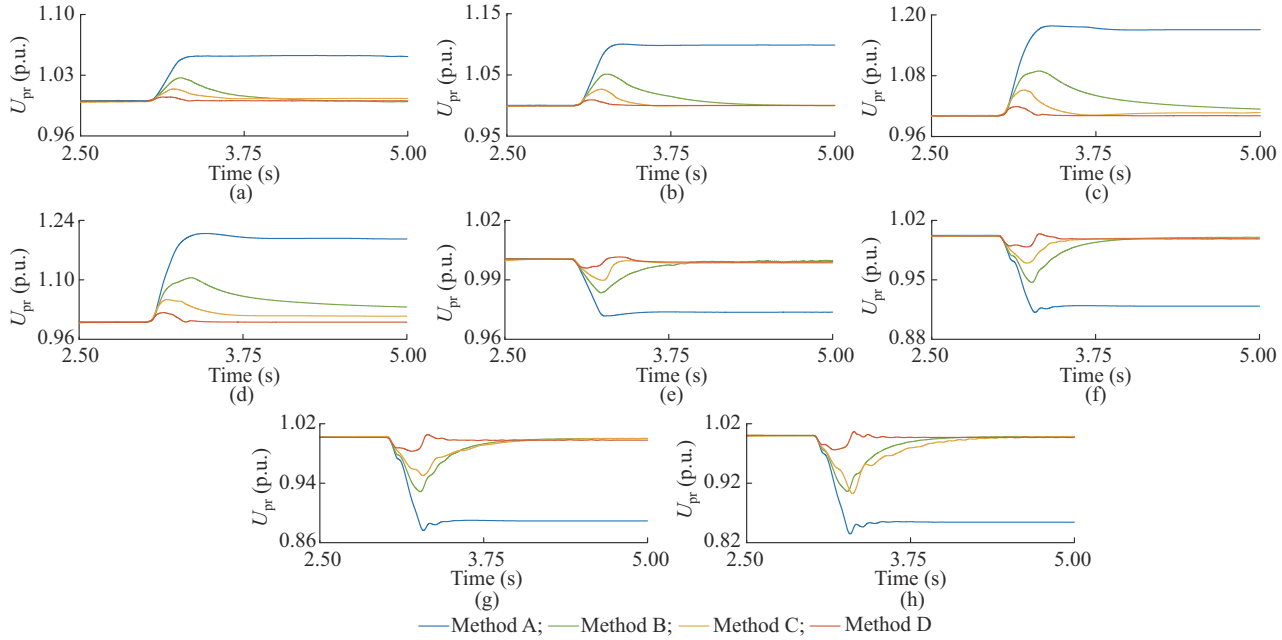

Fig. 6. Simulation results at different fluctuation magnitudes of LCC-HVDC transmission power. (a) U_{pr} with current order decreased from 1.0 p.u. to 0.9 p.u.. (b) U_{pr} with current order decreased from 1.0 p.u. to 0.8 p.u.. (c) U_{pr} with current order decreased from 1.0 p.u. to 0.6 p.u.. (d) U_{pr} with current order decreased from 1.0 p.u. to 0.5 p.u.. (e) U_{pr} with current order increased from 1.0 p.u. to 1.05 p.u.. (f) U_{pr} with current order increased from 1.0 p.u. to 1.15 p.u.. (g) U_{pr} with current order increased from 1.0 p.u. to 1.2 p.u.. (h) U_{pr} with current order increased from 1.0 p.u. to 1.25 p.u..

Referring to Fig. 6(a)-(d), it can be observed that a decrease in the DC current instruction increases U_{pr} across all methods. However, method D can swiftly curtail the maximum voltage to a small value before reinstating it to its nominal value. U_{pr} fluctuation confines within ±0.05 p.u., which indicates that method D exhibits effective control performance across varying degrees of transmission power reduction. Conversely, Fig. 6(e)-(h) illustrates that the minimum value of U_{pr} for all methods decreases with an increase in the order. Despite this, method D displays superior control efficacy compared with the other methods. Additionally, the response speed of method D is faster, and its U_{pr} fluctuation remains within ±0.05 p. u.. These observations demonstrate that method D provides optimal control effectiveness across different magnitudes of transmission power variations.

E. Analysis of Proposed Method with Individual Control Strategy

The proposed method includes control strategies on both the LCC-HVDC and VSC-HVDC sides. Based on the two cases of power increase and power decrease of Sections IV-B and IV-C, this subsection compares the control effects of the LCC side control strategy and the VSC side control strategy as individual controls using the proposed method to further verify the its superiority. The simulation results under the three control methods are shown in Fig. 7, and the comparison of variables under power decrease and increase is presented in Appendix A Table AV.

From Fig. 7 and Table AV, in both cases, methods that utilize only a single LCC or VSC side control are less effective than the proposed method in suppressing voltage disturbances and are slower in addressing unbalanced reactive power. Moreover, compared with method with single control, the magnitude of reactive power adjustment in the proposed method is decreased, meaning that both LCC-HVDC and VSC-HVDC bear less reactive power control burden. The method with single LCC side control, as demonstrated by Fig. 7(d), (f), (j), and (l), mitigates the fluctuation of Q_{dr} during the switching process of DC power modulation, enabling Q_{dr} to change more smoothly, and simultaneously reduces the fluctuation of DC voltage, enhancing the operation characteristics of LCC-HVDC. As shown in Fig. 7(b) and (h), it is evident that single LCC side control also collaboratively reduces the control target of the single VSC side control, alleviating the reactive power control burden on VSC-HVDC.

However, regarding control effect and speed, from Fig. 7(a), (c), (g), and (i), the control response time of the single LCC side control is relatively slow, and its effectiveness in mitigating voltage disturbances is not as good as single VSC side control and the proposed method. From Fig. 7(a), (c), (g), and (i), single VSC side control has a faster response time and a comparatively better voltage disturbance suppression effect, enabling rapid compensation of reactive power. However, from Fig. 7(b), (h), (d), and (j), the VSC-HVDC inverter station has to transfer more reactive power, and the fluctuation of ΔQ_{dr} is larger. The proposed method enhances ΔQ suppression speed through coordinated control, and the magnitudes of Q_{vsc} and ΔQ_{dr} are also decreased. With the AC voltage disturbance being more effectively suppressed, the reactive power provided by the filters is also restored more quickly, further reducing the feedback compensation added to the VSC-HVDC inverter station, presenting an overall virtuous cycle. Thus, lower control burden and higher control efficiency can be achieved through coordination.

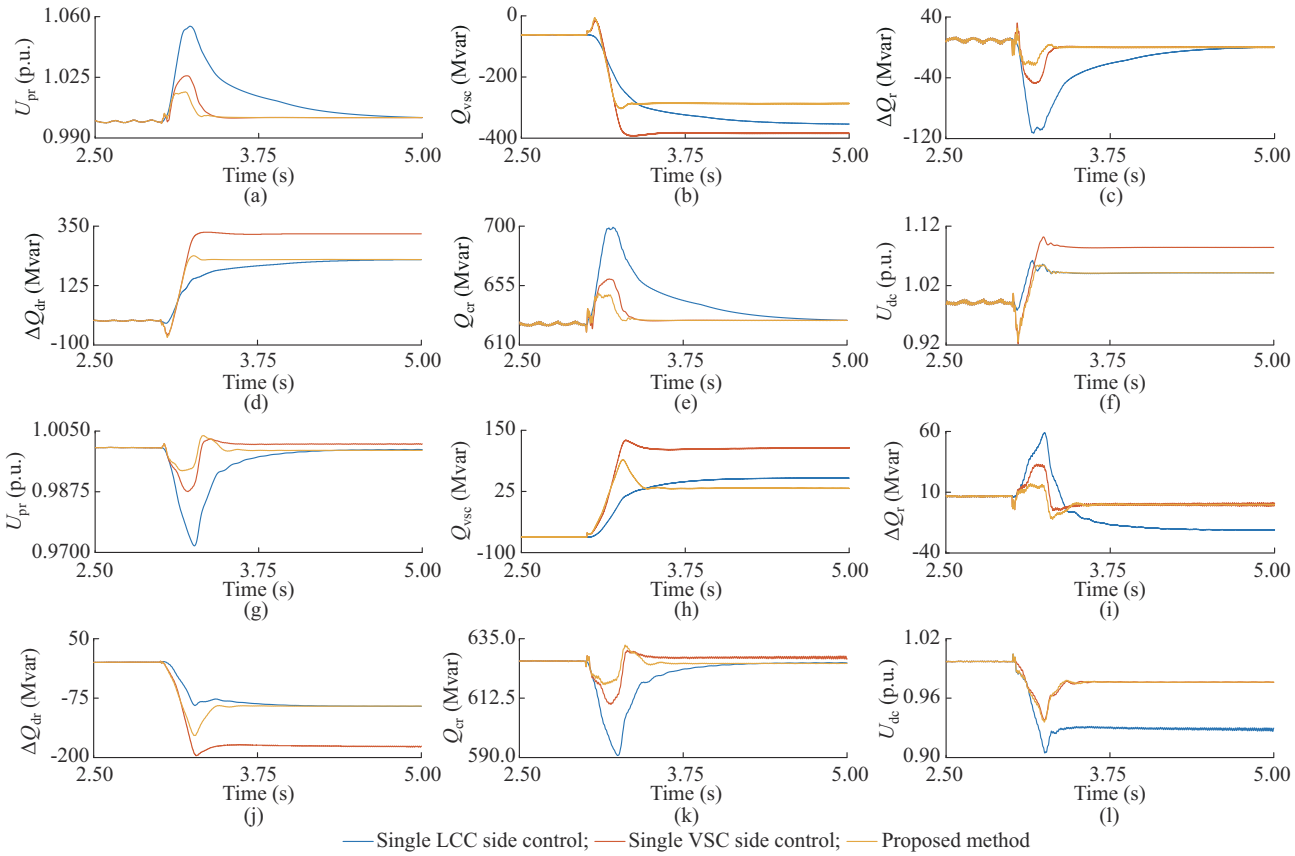

Fig. 7. Simulation results under three control methods. (a) U_{pr} under power decrease. (b) Q_{vsc} under power decrease. (c) ΔQ_r under power decrease. (d) ΔQ_{dr} under power decrease. (e) Q_{cr} under power decrease. (f) U_{dc} under power decrease. (g) U_{pr} under power increase. (h) Q_{vsc} under power increase. (i) ΔQ_r under power increase. (j) ΔQ_{dr} under power increase. (k) Q_{cr} under power increase. (l) U_{dc} under power increase.

F. Analysis of Proposed Method with Different VSC-HVDC Capacities

The capacity of the VSC-HVDC is selected to be 30%, 50%, and 70% of the LCC operation capacity, corresponding to $S_{vsc}=300$ MVA, $S_{vsc}=500$ MVA, and $S_{vsc}=700$ MVA. The analysis aims to evaluate the control effectiveness of the proposed method with different VSC-HVDC capacities. As depicted in Fig. 8, regardless of changes in the VSC-HVDC capacity, the proposed method continues to successfully suppress voltage disturbances. Notably, the suppression effect on U_{pr} disturbances improves as the VSC-HVDC capacity increases. Under the same rated active power output of the VSC-HVDC system, the apparent power ratings differ. The larger the apparent power, the more reactive power the VSC-HVDC can output. Therefore, with the increase of VSC-HVDC capacity, it can provide greater reactive power support during LCC-HVDC power modulation. This outcome indicates that the enhanced capacity of the VSC-HVDC inverter station improves its capability to regulate unbalanced reactive power.

G. Effect of Electrical Distance Between Two Stations on Control Effect

To verify the influence of the electrical distance between the VSC-HVDC inverter station and the LCC-HVDC rectifier station on the proposed method, the electrical distance of the two stations is set to be 20 km, 40 km, and 60 km, and the effectiveness of the proposed method is analyzed under the changing operation conditions of the LCC-HVDC transmission power, respectively. The simulation results with different tie line lengths are presented in Fig. 9.

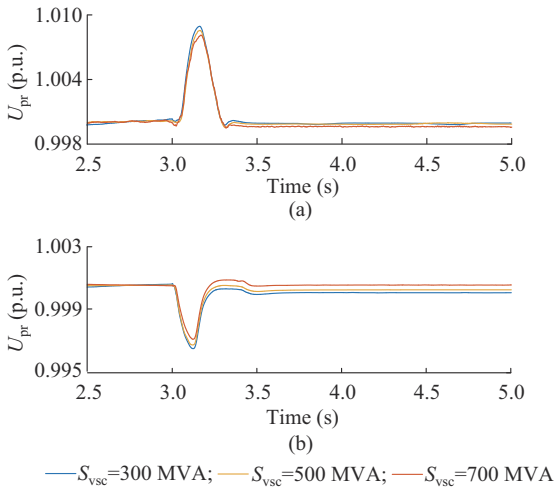

Fig. 8. Simulation results with different VSC-HVDC capacities. (a) PCC voltage under power decrease. (b) PCC voltage under power increase.

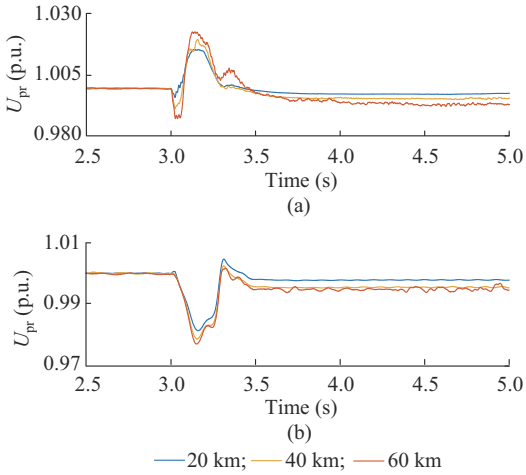

Fig. 9. Simulation results with different tie line lengths. (a) U_{pr} under power decrease. (b) U_{pr} under power increase.

Figure 9 illustrates that the proposed method maintains effective voltage disturbance suppression during variations in the LCC-HVDC transmission power, even when the electrical distance between the two stations changes. As the electrical distance decreases, the proposed method demonstrates enhanced suppression of U_{pr} disturbances. This indicates that a longer electrical distance between the LCC-HVDC and VSC-HVDC systems results in increased tie line losses, thus reducing the influence of the VSC-HVDC system on the LCC-HVDC system. In practical engineering applications, where the LCC-HVDC rectifier station and the VSC-HVDC inverter station are in close proximity, the proposed method can more effectively leverage the benefits of VSC-HVDC to mitigate transient voltage disturbances caused by transmission power fluctuations in LCC-HVDC.

V. Conclusion

The inherent delay of mechanical switch-based reactive power compensators is inadequate to satisfy the increasing variable power transmission demands, leading to power imbalance at the PCC during the switching process of DC power modulation. ΔQ_r and ΔP_r emerge as the primary contributors to voltage disturbance. Consequently, a coordinated feedback power control method for the HMI-HVDC system is proposed to mitigate the AC voltage disturbance at the sending end of LCC-HVDC. By calculating the feedback compensation values for the VSC inverter, the LCC rectifier, and the LCC inverter, the proposed method establishes a closed loop control to regulate the unbalanced power at the PCC based on the quantitative numerical relationship between the unbalanced power and the AC voltage, thus effectively eliminating the unbalanced power exchange.

The proposed method exhibits superior mitigation of AC voltage disturbances. Compared with the traditional control methods, the proposed method comprehensively uses multiple controllable resources, addressing problems of single control and inter-station coordination while lessening the regulatory burden of each power regulation resource.

Appendix A

TABLE AI
Parameters of LCC-HVDC and VSC-HVDC

System	Parameter	Value
LCC-HVDC	Rated power	1000 MW
	Rated AC voltage of sending end	345 kV
	Rated AC voltage of receiving end	230 kV
	Transformer ratio of rectifier	345.0/213.5
	Transformer ratio of inverter	230/209.2
	Rated DC voltage	500 kV
	Rated DC current	2 kA
	Rectifier var compensator	626 Mvar
	Capacity of rectifier transformer	603.73 MVA
	Capacity of inverter transformer	591.8 MVA
	Sending end system SCR	2.5
	X/*R* ratio of grid impedance at rectifier side	9.92
	Receiving end system SCR	3
	Leakage reactance	0.18 p.u.
	Air core reactance	0.20 p.u.
	Knee point voltage	1.25 p.u.
	Tie line reactance	0.03206 Ω/km
	Tie line inductance	0.8984 mH/km
VSC-HVDC	Rated power	450 MVA
	Operation power	400 MW
	Rated voltage of sending end	345 kV
	Rated voltage of receiving end	345 kV
	Transformer ratio of rectifier	345/200
	Transformer ratio of inverter	345/200
	Leakage reactance	0.1 p.u.
	Air core reactance	0.20 p.u.
	Knee point voltage	1.25 p.u.
	Total DC bus capacitance	5000 μF
	Switching frequency	1650 Hz
	Rated voltage	400 kV

TABLE AII
COMPARISON OF VARIABLES UNDER POWER DECREASE

Method	U_{pr} (p.u.)	Peak time (s)	Q_{vsc} (Mvar)	ΔQ_r (Mvar)	ΔQ_{dr} (Mvar)	Q_{cr} (Mvar)	U_{dc} (p.u.)
A	1.143	3.369	–67.4670	–345.485	204.781	882.268	1.222
B	1.073	3.254	–435.012	–126.039	321.070	724.071	1.156
C	1.037	3.221	–437.258	–34.5270	326.484	681.400	1.115
D	1.014	3.157	–309.962	–20.7690	238.056	649.134	1.050

TABLE AIII
COMPARISON OF VARIABLES UNDER POWER INCREASE

Method	U_{pr} (p.u.)	Peak time (s)	Q_{vsc} (Mvar)	ΔQ_r (Mvar)	ΔQ_{dr} (Mvar)	Q_{cr} (Mvar)	U_{dc} (p.u.)
A	0.944	3.281	–69.701	131.542	–56.4930	552.167	0.909
B	0.965	3.267	105.858	83.800	–169.552	581.670	0.906
C	0.985	3.189	134.939	26.585	–199.800	604.940	0.899
D	0.994	3.162	81.193	17.170	–153.520	617.635	0.936

TABLE AIV
AMPLITUDES OF U_{pr} UNDER DIFFERENT FLUCTUATION MAGNITUDES OF TRANSMISSION POWER

Transmission power (p.u.)	U_{pr} (p.u.)			
	Method A	Method B	Method C	Method D
1.25	0.837	0.906	0.903	0.976
1.20	0.877	0.927	0.947	0.982
1.15	0.912	0.946	0.967	0.987
1.05	0.974	0.983	0.989	0.995
0.90	1.053	1.027	1.012	1.005
0.80	1.101	1.052	1.025	1.010
0.60	1.178	1.089	1.048	1.019
0.50	1.209	1.105	1.051	1.023

TABLE AV
COMPARISON OF VARIABLES UNDER POWER DECREASE AND INCREASE

Case	Variable	Single LCC side control	Single VSC side control	Proposed method
LCC-HVDC under power decrease	U_{pr} (p.u.)	1.055	1.0260	1.0170
	Peak time (s)	3.224	3.2020	3.1870
	Q_{vsc} (Mvar)	–354.476	–393.4120	–303.9010
	ΔQ_r (Mvar)	–113.102	–47.6970	–23.6010
	ΔQ_{dr} (Mvar)	223.497	327.3140	238.0550
	Q_{cr} (Mvar)	699.132	659.8650	649.1340
	U_{dc} (p.u.)	1.062	1.1020	1.0550
LCC-HVDC under power increase	U_{pr} (p.u.)	0.972	0.9880	0.9940
	Peak time (s)	3.258	3.2080	3.1640
	Q_{vsc} (Mvar)	52.444	129.8810	89.9960
	ΔQ_r (Mvar)	58.945	33.1110	17.2160
	ΔQ_{dr} (Mvar)	–92.220	–196.2082	–153.5210
	Q_{cr} (Mvar)	590.829	610.1500	617.6350
	U_{dc} (p.u.)	0.938	0.9050	0.9360

REFERENCES

[1] T. Lan, H. Sun, W. Zhong *et al.*, "LCC-HVDC's systematical impact on voltage stability: theoretical analysis and a practical case study," *IEEE Transactions on Power Systems*, vol. 38, no. 2, pp. 1663-1675, Mar. 2023.

[2] H. Rao, C. Zou, S. Xu *et al.*, "The on-site verification of key technologies for Kunbei-Liuzhou-Longmen hybrid multi-terminal ultra HVDC project," *CSEE Journal of Power and Energy Systems*, vol. 8, no. 5, pp. 1281-1289, Sept. 2022.

[3] Z. Suo, H. Li, Z. Yu *et al*., "Research on characteristics and calculation method of HVDC transmission after DC power fast ramp," *Power System Technology*, vol. 42, no. 12, pp. 3833-3841, Dec. 2018.

[4] W. Du, Y. Luo, Y. Li *et al.*, "Reviews of transient overvoltage problem cause by extra reactive power in large scale wind power systems," *Proceedings of the CSEE*, vol. 42, no. 9, pp. 3224-3239, Sept. 2022.

[5] P. Meng, W. Xiang, Y. He *et al.*, "Coordination control of wind farm integrated cascaded hybrid HVDC system in weak grids," *IEEE Transactions on Power Delivery*, vol. 38, no. 3, pp. 1837-1847, Jun. 2023.

[6] D. Li, M. Sun, and Y. Fu, "A general steady-state voltage stability analysis for hybrid multi-infeed HVDC systems," *IEEE Transactions on Power Delivery*, vol. 36, no. 3, pp. 1302-1312, Jun. 2021.

[7] B. Rehman, C. Liu, H. Li *et al.*, "Analysis on local and concurrent commutation failure of multi-infeed HVDC considering inter-converter interaction," *Journal of Modern Power Systems and Clean Energy*, vol. 10, no. 4, pp. 1050-1059, Jul. 2022.

[8] J. Liu, S. Lin, W. Zhong *et al.*, "Improved identification method and fault current limiting strategy for commutation failure in LCC-HVDC," *Journal of Modern Power Systems and Clean Energy*, vol. 10, no. 6, pp. 1761-1772, Nov. 2022.

[9] Q. Xie, X. Xiao, Z. Zheng *et al.*, "An improved reactive power control strategy for LCC-HVDC to mitigate sending end transient voltage disturbance caused by commutation failures," *International Journal of Electrical Power & Energy Systems*, vol. 146, p. 108706, Mar. 2023.

[10] S. Gao, Y. Chen, S. Huang *et al.*, "Efficient power flow algorithm for AC/MTDC considering complementary constraints of VSC's reactive power and AC node voltage," *IEEE Transactions on Power Systems*, vol. 36, no. 3, pp. 2481-2490, May 2021.

[11] H. Xiao, X. Duan, Y. Zhang *et al.*, "Analytically quantifying the impact of strength on commutation failure in hybrid multi-infeed HVDC systems," *IEEE Transactions on Power Electronics*, vol. 37, no. 5, pp. 4962-4967, May 2022.

[12] J. Li, Y. Xia, W. Yao *et al.*, "Reactive power coordinated control for improving transient characteristics of DC side of LCC-HVDC using parallel VSC-HVDC," *Power System Technology*, vol. 46, no. 1, pp. 101-110, Jan. 2022.

[13] Y. Shu, G. Tang, and H. Pang, "A back-to-back VSC-HVDC system of Yu-E power transmission lines to improve cross-region capacity," *CSEE Journal of Power and Energy Systems*, vol. 6, no. 1, pp. 64-71, Mar. 2020.

[14] C. Guo, S. Yang, W. Liu *et al.*, "Single-input-single-output feedback control model and stability margin analysis for hybrid dual-infeed HVDC system," *IEEE Journal of Emerging and Selected Topics in Power Electronics*, vol. 9, no. 3, pp. 3061-3071, Jun. 2021.

[15] H. Xiao, X. Duan, Y. Zhang *et al.*, "Analytically assessing the effect of strength on temporary overvoltage in hybrid multi-infeed HVDC systems," *IEEE Transactions on Power Electronics*, vol. 37, no. 3, pp. 2480-2484, Mar. 2022.

[16] L. Yang, Y. Li, Z. Li *et al.*, "A simplified analytical calculation model of average power loss for modular multilevel converter," *IEEE Transactions on Industrial Electronics*, vol. 66, no. 3, pp. 2313-2322, Mar. 2019.

[17] J. Li, Y. Xia, W. Yao *et al.*, "A coordination control strategy participating in frequency control for VSC-HVDC and LCC-HVDC," in *Proceedings of 2022 IEEE 5th International Electrical and Energy Conference*, Nangjing, China, May 2022, pp. 4716-4721.

[18] T. Li, Y. Li, and Y. Zhu, "Research on the voltage supporting capability of multi-VSC-HVDC subsystems operation strategy to receiving-end LCC-HVDC network in weak AC grid," *CES Transactions on Electrical Machines and Systems*, vol. 7, no. 1, pp. 11-20, Mar. 2023.

[19] X. Ni, A. M. Gole, C. Zhao *et al.*, "An improved measure of AC system strength for performance analysis of multi-infeed HVDC systems including VSC and LCC converters," *IEEE Transactions on Power Delivery*, vol. 33, no. 1, pp. 169-178, Feb. 2018.

[20] H. Yin, X. Zhou, Y. Liu *et al.*, "Interaction mechanism analysis and additional damping control for hybrid multi-infeed HVDC system," *IEEE Transactions on Power Delivery*, vol. 37, no. 5, pp. 3904-3916, Oct. 2022.

[21] Y.-K. Kim, G.-S. Lee, C.-K. Kim *et al.*, "An improved AC system

strength measure for evaluation of power stability and temporary overvoltage in hybrid multi-infeed HVDC Systems," *IEEE Transactions on Power Delivery*, vol. 37, no. 1, pp. 638-649, Feb. 2022.
[22] Y. Zhang and A. M. Gole, "Quantifying the contribution of dynamic reactive power compensators on system strength at LCC-HVDC converter terminals," *IEEE Transactions on Power Delivery*, vol. 37, no. 1, pp. 449-457, Feb. 2022.
[23] Y. Lei, T. Li, Q. Tang *et al.*, "Comparison of UPFC, SVC and STATCOM in improving commutation failure immunity of LCC-HVDC systems," *IEEE Access*, vol. 8, pp. 135298-135307, Feb. 2020.
[24] G.-S. Lee, D.-H. Kwon, and S.-I. Moon, "DC current and voltage droop control method of hybrid HVDC systems for an offshore wind farm connection to enhance AC voltage stability," *IEEE Transactions on Energy Conversion*, vol. 36, no. 1, pp. 468-479, Mar. 2021.
[25] G.-S. Lee, D.-H. Kwon, S.-I. Moon *et al.*, "Reactive power control method for the LCC rectifier side of a hybrid HVDC system exploiting DC voltage adjustment and switched shunt device control," *IEEE Transactions on Power Delivery*, vol. 35, no. 3, pp. 1575-1587, Jun. 2020.
[26] Z. Liu and X. Guo, "Control strategy optimization of voltage source converter connected to various types of AC systems," *Journal of Modern Power Systems Clean Energy*, vol. 9, no. 1, pp. 77-84, Jan. 2021.
[27] J. Li, Y. Xia, C. Yan *et al.*, "A reactive power coordination control scheme for hybrid multi-infeed HVDC system," in *Proceedings of 2020 IEEE Sustainable Power and Energy Conference (iSPEC)*, Chengdu, China, Nov. 2020, pp. 922-927.
[28] X. Zeng, T. Liu, S. Wang *et al.*, "Coordinated transient reactive power control strategy for transmission system connected by VSC-HVDC and LCC-HVDC under commutation failure," *Electric Power Automation Equipment*, vol. 39, no. 12, pp. 28-35, Dec. 2019.
[29] H. Chen, Z. Wang, Z. Yang *et al.*, "Coordinated reactive power control approach for LCC-HVDC and VSC-HVDC in hybrid parallel HVDC system," *Power System Technology*, vol. 41, no. 6, pp. 1719-1725, Jun. 2017.
[30] Q. Xie, Z. Zheng, X. Xiao *et al.*, "Enhancing HVRT capability of DFIG-based wind farms using cooperative rotor-side SMES considering the blocking fault of LCC-HVDC system," *CSEE Journal of Power Energy Systems*, vol. 7, no. 4, pp. 698-707, Jul. 2021.
[31] C. Yin and F. Li, "Reactive power control strategy for inhibiting transient overvoltage caused by commutation failure," *IEEE Transactions on Power Systems*, vol. 36, no. 5, pp. 4764-4777, Sept. 2021.
[32] Q. Xie, Z. Zheng, Y. Wang *et al.*, "Analysis of transient voltage disturbances in LCC-HVDC sending systems caused by commutation failures," *IEEE Transactions on Power Delivery*, vol. 37, no. 5, pp. 4370-4381, Oct. 2022.
[33] R. Liu, J. Yao, X. Wang *et al.*, "Dynamic stability analysis and improved LVRT schemes of DFIG-based wind turbines during a symmetrical fault in a weak grid," *IEEE Transactions on Power Electronics*, vol. 35, no. 1, pp. 303-318, Jan. 2020.
[34] X. Deng, S. Wang, Y. Shen *et al.*, "Main circuit parameter design of Zhundong-Sichuan ±1100 kV UHVDC power transmission project," *Electric Power Automation Equipment*, vol. 34, no. 4, pp. 133-140, Apr. 2014.
[35] M. O. Faruque, Y. Zhang, and V. Dinavahi, "Detailed modeling of CIGRE HVDC benchmark system using PSCAD/EMTDC and PSB/SIMULINK," *IEEE Transactions on Power Delivery*, vol. 21, no. 1, pp. 378-387, Jan. 2006.
[36] X. Wang, X. Li, W. Wei *et al.*, "Coordinated control strategy for interconnected transmission system of VSC-HVDC and LCC-HVDC," *Electric Power Automation Equipment*, vol. 36, no. 12, pp. 102-108, Dec. 2016.

Jiachen Zhang received the B.S. degree in electrical engineering from China University of Petroleum (East China), Qingdao, China, in 2022. He is currently pursuing the Master's degree in electrical engineering with Sichuan University, Chengdu, China. His main research interests include renewable energy and high-voltage direct current (HVDC).

Qi Xie received the B.S. degree in electrical engineering and its automation in 2019 from Sichuan University, Chengdu, China, where he is currently working toward the Ph.D. degree in electrical engineering. His research interests include renewable energy and HVDC.

Zixuan Zheng received the B.S. and Ph.D. degrees in electrical engineering from Sichuan University, Chengdu, China, in 2012 and 2017, respectively. He is currently working as an Associate Professor in the College of Electrical Engineering, Sichuan University. His research interests include power quality, and operation and control of distributed energy resources.

Chunyi Guo received the B.S. and Ph.D. degrees in power system and automation from North China Electric Power University (NCEPU), Beijing, China, in 2007 and 2012, respectively. He is currently a Professor at NCEPU. His research interests include HVDC and power electronics.

Yi Zou received the B.S. degree in electrical engineering from Sichuan University, Chengdu, China, in 2022. She is currently pursuing the Master's degree in electrical engineering with Sichuan University. Her main research interests include renewable energy and HVDC.

Jie Ren received the B.S. and Ph.D. degrees in electrical engineering from Sichuan University, Chengdu, China, in 2017 and 2022, respectively. She is currently a Lecturer with the College of Electrical Engineering, Sichuan University. Her research interests include renewable energy generation and fault ride through of wind turbine generator.